

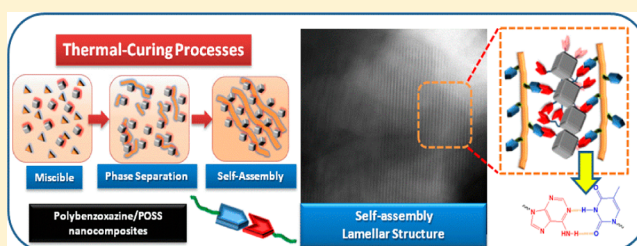
# Complementary Multiple Hydrogen Bonding Interactions Induce the Self-Assembly of Supramolecular Structures from Heteronucleobase-Functionalized Benzoxazine and Polyhedral Oligomeric Silsesquioxane Nanoparticles

Wei-Hsun Hu, Kai-Wei Huang, Chin-Wei Chiou, and Shiao-Wei Kuo\*

Department of Materials and Optoelectronic Science, Center for Nanoscience and Nanotechnology, National Sun Yat-Sen University, Kaohsiung 804, Taiwan

## Supporting Information

**ABSTRACT:** We prepared octuply adenine (A)-functionalized polyhedral oligomeric silsesquioxane [(octakis(vinylbenzyladenine-siloxy)silsesquioxane, OBA-POSS)] nanoparticles through the reaction of A with octakis(benzyl chloride) POSS (OVBC-POSS), itself prepared through hydrosilylation of octakis(dimethylsiloxy)-silsesquioxane ( $Q_8M_8^H$ ) with vinyl benzyl chloride. We observed the self-assembly of lamellar structures from the complexation of a thymine (T)-functionalized polybenzoxazine (PA-T) with OBA-POSS, stabilized through complementary multiple hydrogen bonding interactions between the T groups of PA-T and the A groups of OBA-POSS. In addition, incorporating POSS presenting multiple, strong, complementary hydrogen bonding A units into the PA-T matrix significantly enhanced the thermal stability of this polymer, as evidenced using differential scanning calorimetry and thermogravimetric analysis.



## INTRODUCTION

Benzoxazine monomers are heterocyclic compounds featuring an oxazine ring; they are synthesized from a primary amine, phenol, and formaldehyde. Benzoxazines can be polymerized through ring-opening polymerization in the absence of a catalyst, releasing no byproducts.<sup>1</sup> The advantageous properties of benzoxazine resins include near-zero shrinkage upon polymerization, low water absorption, high char yield, excellent dimensional stability, flame retardance, stable dielectric constants, and low surface free energy.<sup>2</sup>

Procedures for the modification of benzoxazine resins are growing rapidly, with many useful products having been developed in recent years.<sup>3</sup> To improve the performance of polybenzoxazines (PBZs), polymerizable alkynyl and allyl side groups have been introduced into benzoxazine monomers.<sup>4</sup> Benzoxazine resins have also been modified through blending with other polymers [e.g., epoxy, polyurethane, poly(*N*-vinyl-2-pyrrolidone)],<sup>5</sup> inorganic species (e.g., clays),<sup>6</sup> polyhedral oligomeric silsesquioxane (POSS),<sup>7</sup> and carbon nanotubes.<sup>8</sup> Unlike clay or conventional fillers, POSS has a monodisperse molecular weight, a well-defined structure, low density, high temperature stability, an absence of trace metals, and sizable interfacial interactions between its composite particle and polymer segments.<sup>71</sup> As a result, highly functionalized benzoxazine or epoxy POSS monomers have been employed widely to prepare covalently bonded PBZ/POSS nanocomposites.<sup>7</sup> In general, these kinds of PBZ/POSS nanocomposites exhibit featureless morphologies, with no discernible phase separation, suggesting that the POSS nanoparticles are dispersed homogeneously throughout the matrix. Functionalizing polymers with nucleic acid bases

(DNA bases) allows the formation of complexes stabilized through multiple hydrogen bonding interactions with complementary bases. Multiple hydrogen bonding arrays play a fundamental role in complex biological systems (e.g., DNA complexation); they are influential structures in polymer science, where they are often presented as defined macromolecules possessing near-perfect molecular structures.<sup>9</sup> As a result, the preparation of synthetic polymers that mimic DNA remains an important challenge in polymer science.<sup>10</sup> Chang et al. prepared a benzoxazine derivative with supramolecular functionality (i.e., a uracil unit) through the reaction of a uracil-functionalized amine with phenol and formaldehyde.<sup>11</sup> In addition, we have also synthesized a thymine (T)-functionalized benzoxazine (PA-T) through Michael addition of T to an acryloyl-functionalized benzoxazine (Pa-Ac).<sup>12</sup>

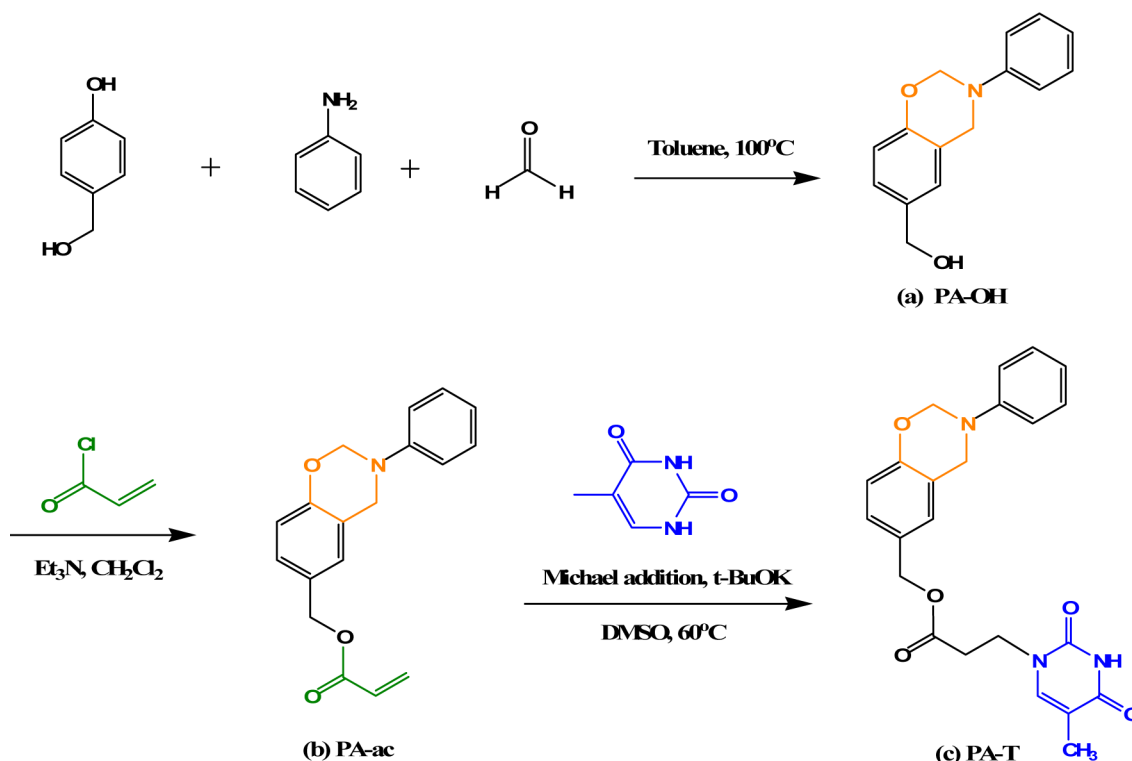
In this study, we synthesized a new octuply adenine (A)-functionalized POSS-based material and then blended it with a thymine (T)-functionalized PBZ (PA-T) to form PBZ/POSS nanocomposites. First, we produced octakis(benzyl chloride) POSS (OVBC-POSS) through hydrosilylation (Scheme 1a) of vinylbenzyl chloride (VBC) with octakis(dimethylsiloxy)-silsesquioxane ( $Q_8M_8^H$ ); we then synthesized the star-shaped octuply A-functionalized POSS [octakis(vinylbenzyladenine-siloxy)silsesquioxane, OBA-POSS] from the reaction of OVBC-POSS with A (Scheme 1b). We used Fourier transform infrared

Received: October 3, 2012

Revised: November 4, 2012

Published: November 14, 2012

Scheme 1. Synthesis of (a) PA-OH, (b) PA-ac, and (c) PA-T



(FTIR) spectroscopy and transmission electron microscopy (TEM) to characterize the supramolecular structures self-assembled through multiple hydrogen bonding interactions between PA-T and OBA-POSS. In addition, we found that the octuply A-functionalized POSS imparted PA-T with surprising aggregation stability as a result of the formation of multiple hydrogen bonded pairs. The resulting self-assembly of supramolecular lamellae based on molecular recognition between complementary components led to a morphology similar to that for the microphase separation of block copolymers in the bulk state. This approach should allow the synthesis of a wide range of self-assembled supramolecular structures with specified degrees of internal organization.

## EXPERIMENTAL SECTION

**Materials.** Octakis(dimethylsiloxy)silsesquioxane ( $\text{Q}_8\text{M}_8^{\text{H}}$ ) containing eight hydrosilane groups was obtained from Hybrid Plastics. Paraformaldehyde, acryloyl chloride, and 4-hydroxybenzyl alcohol were purchased from Aldrich. Potassium *tert*-butoxide, T, and A were obtained from Showa (Japan). Vinylbenzyl chloride, dimethylformamide (DMF), toluene, and dimethyl sulfoxide (DMSO) were purchased from Acros Organics (Germany) and distilled from  $\text{CaH}_2$  under vacuum prior to use. Sodium hydride in oil (57–63%) was purchased from Alfa. All other chemicals were of reagent grade and used as received without further purification. The benzoxazine monomer (3-phenyl-3,4-dihydro-2H-benzo[e][1,3]-oxazin-6-yl)methylthymine (PA-T) was prepared as previously reported, and the chemical reaction is summarized in Scheme 1.<sup>12</sup>

**Octakis(vinylbenzyladenine-siloxy)silsesquioxane (OBA-POSS).** A solution of  $\text{Q}_8\text{M}_8^{\text{H}}$  (1.00 g, 0.980 mmol) and vinyl benzyl chloride (1.20 g, 7.86 mmol) in toluene (50 mL) was heated at 60 °C under Ar, and then Pt(dvs) (0.07 mL, 0.13 mmol) was added via syringe. After stirring for 4 h, the Pt(dvs) catalyst was removed by passing the mixture through activated charcoal.<sup>7i,10i,13</sup> The solvent was evaporated in a rotary evaporator to give OVBC-POSS as a viscous liquid [ $^{29}\text{Si}$  NMR (ppm):  $\delta$  12.16 [( $\text{CH}_3$ )<sub>2</sub>SiCH<sub>2</sub>CH<sub>2</sub>], 10.28 [( $\text{CH}_3$ )<sub>2</sub>Si(CH<sub>2</sub>CH<sub>3</sub>)], -109.2 [SiOSi(CH<sub>3</sub>)<sub>2</sub>H]]. Subsequently, a solution of A (0.53 g, 3.9 mmol)

and  $\text{K}_2\text{CO}_3$  (0.49 g, 3.9 mmol) in DMF (50 mL) was stirred at ambient temperature for 4 h, then OVBC-POSS (1.0 g, 0.45 mmol) was added, and the mixture was then stirred at 80 °C for 24 h. After removing the solvents under reduced pressure, the residue was dissolved in THF and the salts were removed using a neutral alumina column. A yellowish viscous liquid was obtained (55%) after drying in a vacuum oven overnight at room temperature. The chemical reaction is summarized in Scheme 2. MALDI-TOF mass (Figure S1, calcd 2947).  $^1\text{H}$  NMR (DMSO, ppm):  $\delta$  5.31 (s, 2H), 8.16 (s, 2H,  $\text{NH}_2$ ), 8.22 (s, 1H), 3.54 (s, 2H).  $^{13}\text{C}$  NMR (DMSO, ppm):  $\delta$  45.9, 118.7, 144.1, 149.5, 152.6, 156.0. FTIR (KBr,  $\text{cm}^{-1}$ ): 3317, 3157 (NH str), 2959, 2844 (aliphatic CH str), 1062 (SiOSi), 1652 (C=N str), 1601 (NH def). Elemental analysis: Anal. Calcd for OBA-POSS C, 44.18; H, 3.94; N, 18.41. Found: C, 56.82; H, 6.49, N, 19.40.

**PA-T/OBA-POSS Nanocomposites.** Solutions of desired amounts of PA-T and OBA-POSS in THF were mixed and stirred for 2 h at room temperature, poured onto an Al plate, dried for 6 h in the open air, and then placed in an oven at 100 °C under vacuum for 2 h. The cast film was polymerized in a stepwise manner: at 140 and 160 °C for 3 h each and then at 200 °C for 4 h. Each cured sample was transparent and had a dark red color.

**Characterization.**  $^1\text{H}$  and  $^{13}\text{C}$  nuclear magnetic resonance (NMR) spectra were recorded using an INOVA 500 instrument with  $\text{CDCl}_3$  as solvent and TMS as the external standard; chemical shifts are reported in parts per million (ppm). FTIR spectra of the polymer blend films were recorded using the conventional KBr disk method with a Bruker Tensor 27 FTIR spectrophotometer (32 scans; spectral resolution, 1  $\text{cm}^{-1}$ ); the films were sufficiently thin to obey the Beer–Lambert law. DSC was performed using a TA-Q20 instrument operated at a scan rate of 20 °C/min over a temperature range from 0 to 250 °C under a  $\text{N}_2$  atmosphere. The thermal stability of the samples was characterized using a TA Q-50 thermogravimetric analyzer operated under a  $\text{N}_2$  atmosphere. The cured sample (ca. 7 mg) was placed in a Pt cell and heated at a rate of 20 °C/min from 30 to 800 °C at a  $\text{N}_2$  flow rate of 60 mL/min. TEM was conducted using a JEOL 2100 microscope (Japan) operated at 200 kV. Ultrathin sections of the samples were prepared using a Leica Ultracut S microtome equipped with a diamond knife; slices (thickness: ca. 700 Å) were cut at room

**Scheme 2. Synthesis of OBA-POSS: (a)  $Q_8M_8^H$  Hydrosilylation with VBC To Form (b) OVBC-POSS and Subsequent Reaction with A To Form OBA-POSS**

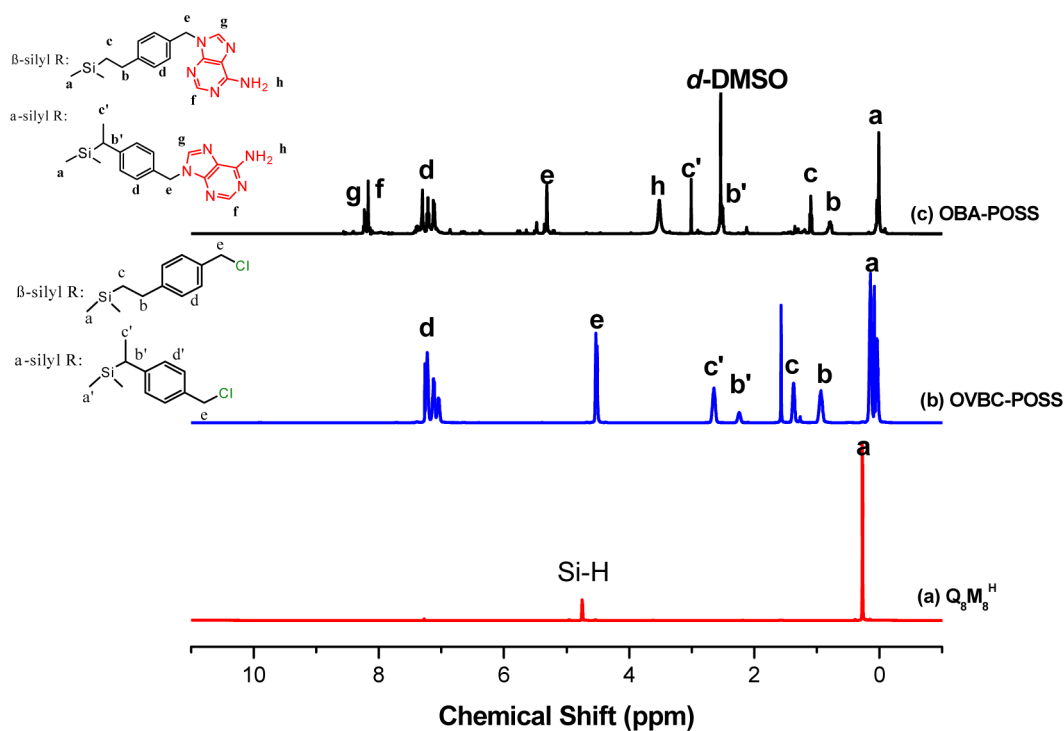
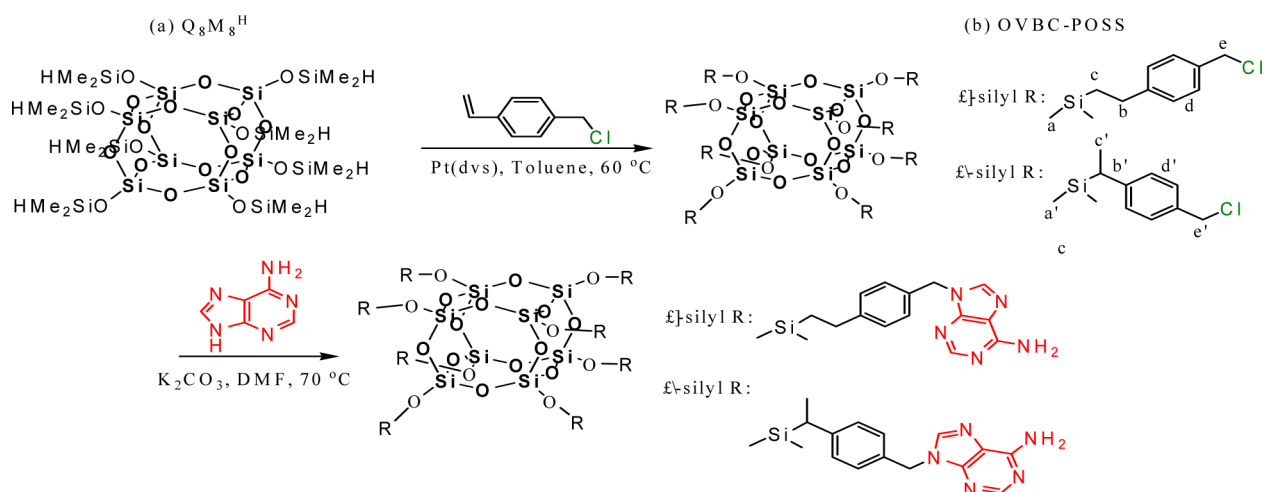


**Figure 1.**  $^1H$  NMR spectra of (a)  $Q_8M_8^H$ , (b) OVBC-POSS in  $CDCl_3$ , and (c) OBA-POSS in  $d_6$ -DMSO.

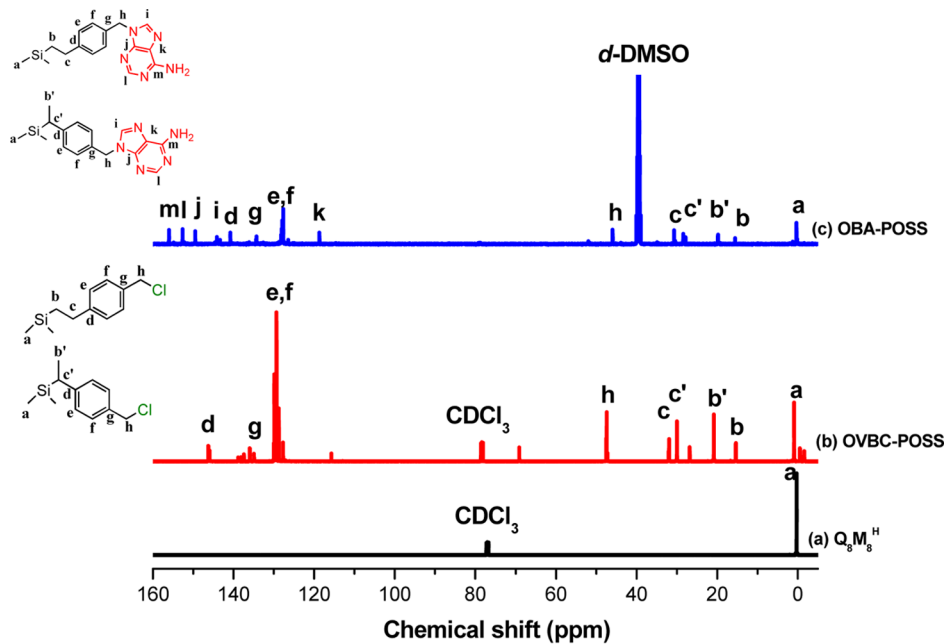
temperature. Nanoindentation tests were performed using an XP Nano Indenter (MTS, Nano Instruments Innovation Center, Oak Ridge, TN), a three-sided pyramid (Berkovich) diamond indenter, and a continuous stiffness measurement (CSM) technique.

## RESULTS AND DISCUSSION

**Synthesis of OBA-POSS.** Figure 1 displays  $^1H$  NMR spectra of  $Q_8M_8^H$ , OVBC-POSS, and OBA-POSS. The signal for the Si–H units (4.7 ppm) of  $Q_8M_8^H$  (Figure 1a) was absent in the spectrum of OVBC-POSS (Figure 1b), confirming complete hydrosilylation. The latter spectrum reveals that the vinyl groups of VBC underwent hydrosilylation of the Si–H bonds of  $Q_8M_8^H$  in both  $\alpha$  and  $\beta$  configurations (i.e., a mixture of these two orientations exists). We determined the ratio of  $\beta$  to  $\alpha$  linkages (1.64:1) for OVBC-POSS through integration of the

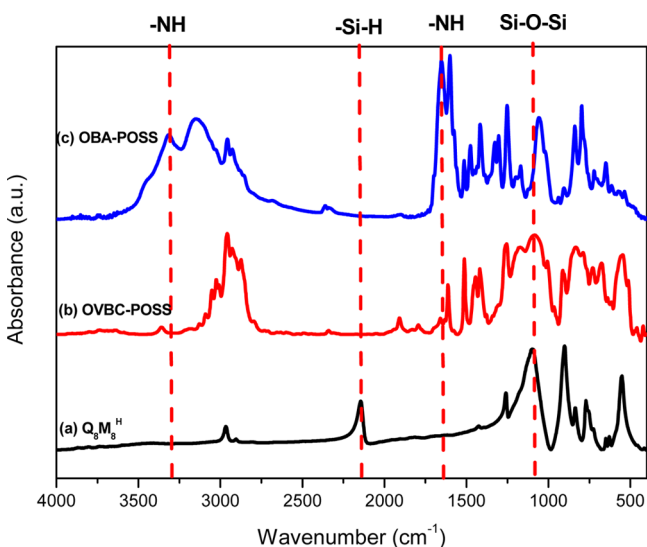
signals for the protons marked  $b$  (2H,  $\beta$ -side groups) and  $b'$  (1H,  $\alpha$ -side groups).<sup>7i,10i,13</sup> The complete substitution of chloride atoms by A groups was confirmed in the  $^1H$  NMR spectrum of OBA-POSS (Figure 1c); the signal for the benzylic  $CH_2Cl$  groups (4.50 ppm) shifted to 4.31 ppm for the corresponding T-substituted benzylic moieties. The absence of any remnant resonance at 4.50 ppm suggested that the substitution had reached completion under the reaction conditions.

Figure 2 displays the  $^{13}C$  NMR spectra of  $Q_8M_8^H$ , OVBC-POSS, and OBA-POSS. The signal for the benzylic carbon nucleus (C-h) of OVBC-POSS at 47.2 ppm (Figure 2b) shifted to 45.8 ppm after substitution with A (Figure 2c). The methyl and methylene signals of OVBC-POSS remained in the spectrum of OBA-POSS (0.2, 15.2, 20.7, 29.9, and 31.8 ppm).



**Figure 2.**  $^{13}\text{C}$  NMR spectra of (a)  $\text{Q}_8\text{M}_8^{\text{H}}$ , (b) OVBC-POSS in  $\text{CDCl}_3$ , and (c) OBA-POSS in  $d_6$ -DMSO.

Figure 3 presents FTIR spectra of  $\text{Q}_8\text{M}_8^{\text{H}}$ , OVBC-POSS, and OBA-POSS, recorded at room temperature. The strong absorption



**Figure 3.** FTIR spectra of (a)  $\text{Q}_8\text{M}_8^{\text{H}}$ , (b) OVBC-POSS, and (c) OBA-POSS.

peaks near  $1100\text{ cm}^{-1}$  for all compounds represented the vibrations of the siloxane Si–O–Si groups—a general feature of POSS derivatives. The characteristic stretching vibrations of the Si–H groups appeared as a signal at  $2200\text{ cm}^{-1}$  in Figure 3a. In the spectrum of OVBC-POSS (Figure 3b), this peak was completely absent, indicating that the reaction had reached completion. After the substitution reaction, the spectrum of OBA-POSS (Figure 3c) featured signals at  $3317$ ,  $3157$ ,  $1652$ , and  $1601\text{ cm}^{-1}$ , corresponding to N–H stretching and bending of the A groups. Thus, the  $^1\text{H}$  and  $^{13}\text{C}$  NMR and FTIR spectroscopic analyses were all indicative of the successful synthesis of OBA-POSS.

**Thermal Properties of PA-T/OBA-POSS Nanocomposites.** Figure S2 displays the macroscopic morphologies for our

PBZ/POSS composites. The composites of the PA-T monomer with both  $\text{Q}_8\text{M}_8^{\text{H}}$  and OBA-POSS were soluble in THF. The mixtures were poured onto an Al plate; after evaporation of the solvent, the samples were cured in air in an oven. The PA-T/ $\text{Q}_8\text{M}_8^{\text{H}}$  composites (which lack complementary multiple hydrogen bonding interactions) were cloudy and friable both before (Figure S2a) and after (Figure S2c) thermal curing, suggesting that the  $\text{Q}_8\text{M}_8^{\text{H}}$  units aggregated considerably during the thermal curing process. In contrast, the mixtures of PA-T and OBA-POSS (i.e., with complementary multiple hydrogen bonding interactions) were all homogeneous and transparent, suggesting that the two components were completely miscible in the composition range investigated (Figure S2b); all of their cured samples were transparent and were colored dark red (Figure S2d).

FTIR spectroscopy is a highly effective tool for investigating hydrogen bonding interactions in supramolecular arrays. The presence of multiple hydrogen bonds between the PA-T monomer and OBA-POSS was evident in the FTIR spectra in Figure S3. Figure 4 presents expanded FTIR spectra ( $1800$ – $1500\text{ cm}^{-1}$ ) for various PA-T/OBA-POSS blends prior to thermal polymerization. Analyzing these spectra using the second-derivative technique,<sup>10i,k</sup> we observed five major peaks for pure PA-T: ring vibrations at  $1598\text{ cm}^{-1}$ ; self-complementary multiple T–T hydrogen bonding at  $1641\text{ cm}^{-1}$ ; free C=O groups of T units at  $1671\text{ cm}^{-1}$ ; acetyl C=O groups hydrogen-bonded with the T moieties at  $1710\text{ cm}^{-1}$ ; and free acetyl C=O groups at  $1730\text{ cm}^{-1}$ . The A groups of OBA-POSS provided characteristic signals at  $1657\text{ cm}^{-1}$  (bonded  $\text{NH}_2$  scissor plus ring stretching) and  $1600\text{ cm}^{-1}$  (ring stretching plus bonded  $\text{NH}_2$  scissor). The intensity of signal of the free C=O groups of T at  $1671\text{ cm}^{-1}$  decreased upon increasing the OBA-POSS content in the blend, consistent with the existence of multiple hydrogen bonding interactions between the A and T groups.

We used DSC to examine the glass transition behavior of the PA-T/OBA-POSS nanocomposites after thermal curing (Figure 5). For pure PA-T and pure OBA-POSS, the glass transition temperatures ( $T_g$ ) were  $115$  and  $50\text{ }^\circ\text{C}$ , respectively. Pure PA-T features strong self-complementary multiple hydrogen bonding

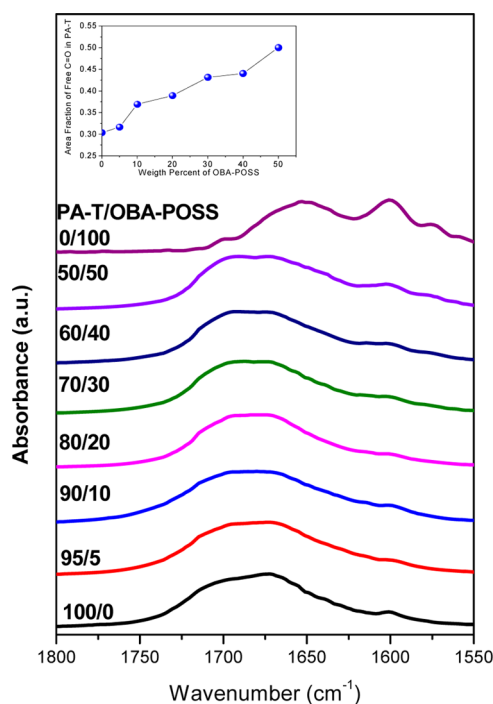


Figure 4. FTIR spectra of the PA-T monomer blended with various OBA-POSS contents at room temperature.

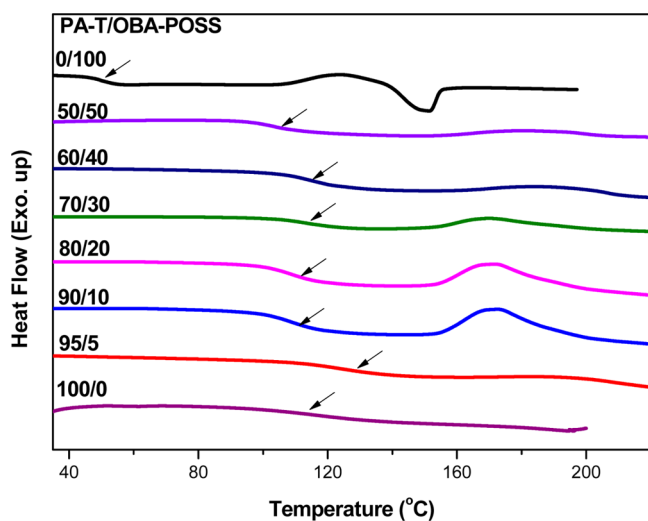


Figure 5. DSC thermograms (second heating runs) of various PA-T/OBA-POSS nanocomposites.

interactions among its T groups, leading to a relatively high value of  $T_g$ .<sup>12</sup> The glass transition temperature of pure OBA-POSS, which also features strong, self-complementary, multiple hydrogen bonding interactions, is higher than that of a similar octakis-functionalized POSS lacking multiple hydrogen bonding interactions.<sup>71</sup> In addition, the exothermic peak at 100–140 °C and the endothermic peak near 150 °C for pure OBA-POSS correspond to crystallization and melting, respectively, of the POSS moieties.<sup>14</sup> This melting temperature was confirmed through small-angle X-ray scattering (Figure S4), where the scattering peak from aggregation of OBA-POSS disappeared completely at 180 °C.

Although the glass transition temperature did not change appreciably upon increasing the OBA-POSS content in the PA-T/

OBA-POSS complexes, it reached its maximum value at an OBA-POSS content of 5 wt %. In previous studies, Lee found<sup>7d–g</sup> that multifunctionalized benzoxazine POSS derivatives at a content of up to 10 wt % in benzoxazine hybrids led to aggregation of the POSS units and, thereby, macro-phase separation, which decreased their overall effectiveness in hindering polymer movement. Thus, multifunctionalized benzoxazine POSS, which features an inorganic silsesquioxane core, appears to undergo considerable aggregation during the thermal curing process. In this present study, we suspected that strong, complementary, multiple hydrogen bonding interactions would exist between the T groups of PA-T and the A groups of OBA-POSS and, therefore, an increase in the glass transition temperature upon increasing the OBA-POSS content in the blend. Alternatively, taking into account the effects of the chain mobility and viscosity of PA-T and OBA-POSS, we might also have expected cross-linking and self-complementary multiple hydrogen bonding to decrease the chain mobility and possibly decrease the degree of interassociation through complementary multiple hydrogen bonding of PA-T with OBA-POSS. Figure 5 reveals, however, that essentially each of our PA-T/OBA-POSS nanocomposites exhibited an exothermic peak in its DSC trace at a temperature above its value of  $T_g$  at higher OBA-POSS contents. We assign this exothermic peak to the enthalpy of complementary hydrogen bond formation.<sup>15</sup> The temperature of this exothermic peak and its enthalpy depended on the DSC heating rate or the number of heating scans, as revealed in Figure 6 for PA-T/OBA-POSS =

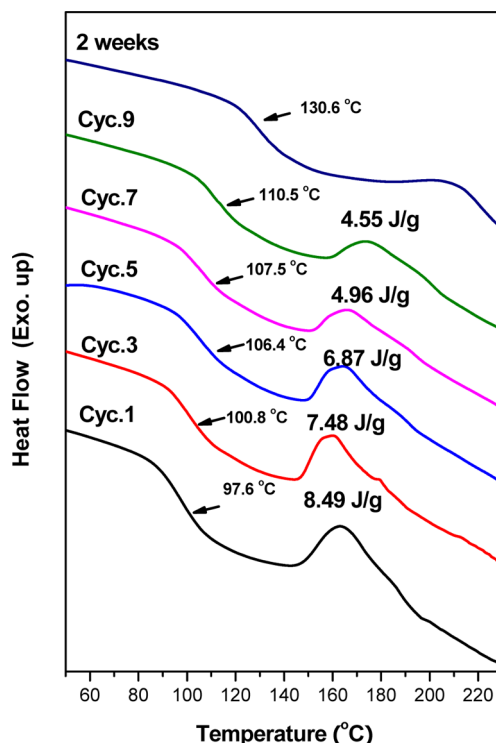


Figure 6. DSC analyses revealing the reversibility of multiple hydrogen bonding in each heating cycles.

80/20. Notably, this exothermic peak did not correspond to thermal polymerization of the PA-T monomer because it exhibited reversible behavior—even after nine heating scans. Nevertheless, the enthalpy of hydrogen bonding formation decreased upon increasing the number of heating scans (Figure 6). Furthermore, when we thermally annealed the sample at 250 °C for

2 weeks and then quickly quenched it to room temperature, the enthalpy of hydrogen bond formation disappeared almost totally during the subsequent heating scan, indicating that the formation of complementary multiple hydrogen bonds was already complete during the cooling process. As a result, the value of  $T_g$  increased by  $\sim 35$  °C after thermal annealing of the PA-T/OBA-POSS complexes (Figure 6).

We speculate that the chain mobility increased at temperatures above the values of  $T_g$  of PA-T and OBA-POSS, with rearrangement of the chains' conformations allowing more intimate mixing and providing more appropriate orientations at the interassociation sites (i.e., the T groups of PA-T and the A groups of OBA-POSS). This result is similar to that observed for the high glass transition temperatures of polymer blends of poly(vinylphenol) (PVPh) and poly(methyl methacrylate) (PMMA),<sup>16</sup> where it is concluded that even though hydrogen bonding between PVPh and PMMA favors their miscibility, phase separation still occurs, resulting in a nonequilibrium multiphase system that is effectively frozen; nevertheless, thermal treatment influences the formation of hydrogen bonds again, thereby enhancing the miscibility of PVPh/PMMA blends.

Figure 7 displays DSC thermograms of blends at various PA-T/OBA-POSS ratios after thermal annealing at 250 °C for

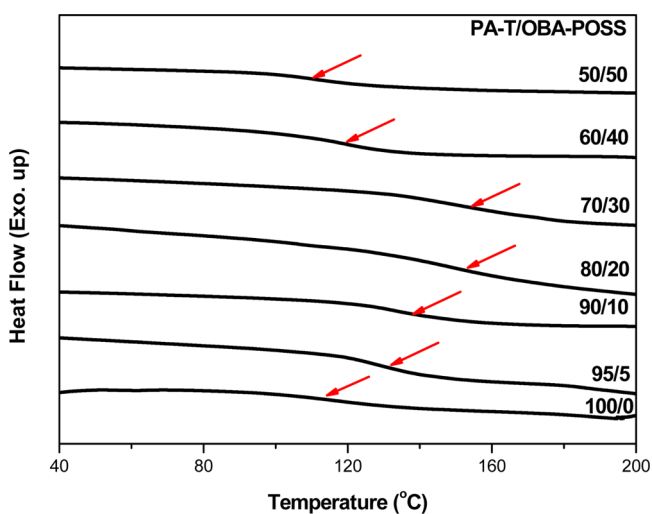


**Figure 7.** DSC thermograms of blends at various PA-T/OBA-POSS ratios after thermal annealing at 250 °C for 2 weeks.

2 weeks and then quickly quenching to room temperature. The exothermic peaks disappeared completely during the subsequent heating scan, with the values of  $T_g$  having increased for all PA-T/OBA-POSS ratios, compared with those prior to thermal annealing.

Figure 8 summarizes the corresponding glass transition temperatures. The Kwei equation<sup>17</sup> is usually employed to characterize systems displaying specific interactions:

$$T_g = \frac{W_1 T_{g1} + kW_2 T_{g2}}{W_1 + kW_2} + qW_1 W_2 \quad (1)$$

where  $W_1$  and  $W_2$  are the weight fractions of the components,  $T_{g1}$  and  $T_{g2}$  are the corresponding glass transition temperatures, and  $k$  and  $q$  are fitting constants. The parameter  $q$  represents the strength of the specific interactions in the system; it reflects a balance between the breaking of self-association interactions and the forming of interassociation interactions. From non-linear least-squares "best fits" of the plots for the PA-T/OBA-POSS

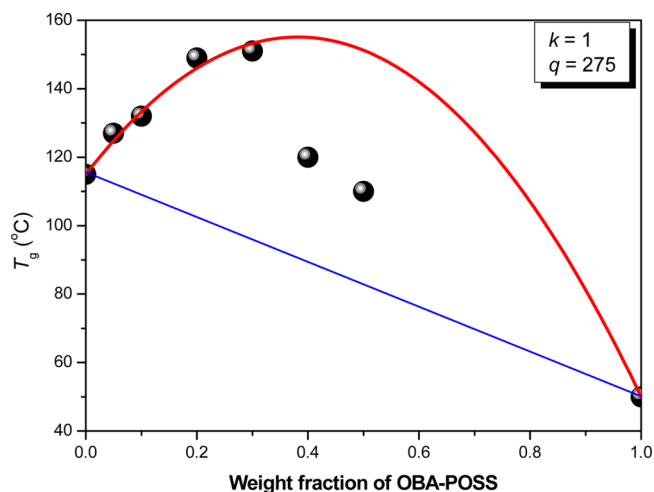


**Figure 8.** Glass transition behavior of PA-T/OBA-POSS nanocomposites, determined using the Kwei equation.

complexes, we obtained values of  $k$  and  $q$  of 1 and 275, respectively. A positive value of  $q$  usually suggests that strong specific intermolecular interactions exist between the two polymers.<sup>18</sup> In Figure 8, the value of  $T_g$  of pure PA-T is 115 °C and those of its blends with OBA-POSS at contents of 5, 10, 20, 30, 40, and 50 wt % are 127, 132, 149, 151, 120, and 110 °C, respectively. Thus, the value of  $T_g$  of the complex increased dramatically upon increasing the OBA-POSS content to 30 wt % (<30 wt % provided a good fit with the Kwei equation) but decreased thereafter (>40 wt % led to a large negative deviation with the Kwei equation). This behavior presumably resulted from two opposing effects of the POSS cages in the PBZ matrix.<sup>71</sup> One, the nanoreinforcement effect of OBA-POSS on the PA-T PBZ matrix, tending to increase the value of  $T_g$  of the blend through complementary multiple hydrogen bonding interactions at relatively low OBA-POSS contents. The other, the inclusion of OBA-POSS, which features an inorganic silsesquioxane core, in the system leading to serious aggregation during the thermal curing process, thereby decreasing the cross-linking density in the network structure and decreasing the values of  $T_g$  at relatively high OBA-POSS contents.

Figure 9 reveals the thermal stabilities of the PA-T/OBA-POSS nanocomposites under  $N_2$ . To compare the thermal stabilities,

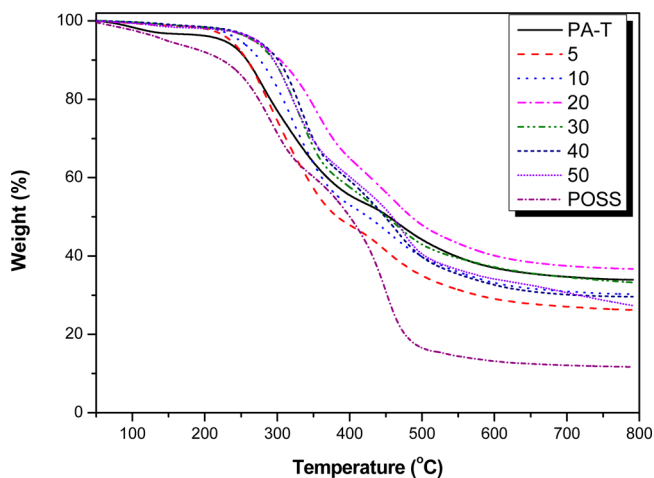


**Figure 9.** TGA analyses of PA-T/OBA-POSS blends incorporating different amounts of OBA-POSS.

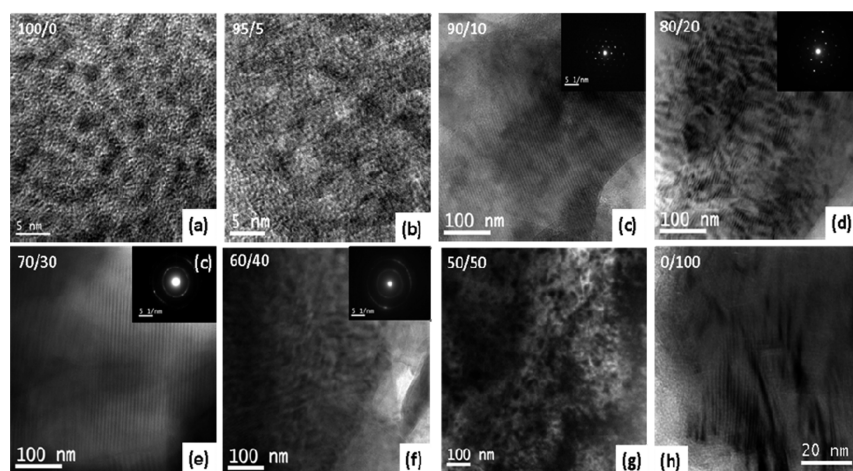


**Figure 10.** TEM images and SAED patterns of PA-T/OBA-POSS blends incorporating different amounts of OBA-POSS.

here we use the 10 wt % weight loss temperature as a standard. The decomposition temperature ( $T_d$ ) of the PA-T/OBA-POSS nanocomposites gradually increased upon increasing the OBA-POSS content up to 20 wt %; further increases in the OBA-POSS content caused the decomposition temperature to decrease, due to a phenomenon similar to that for the trend in the values of  $T_g$ . The variation in thermal stability, as measured in terms of the decomposition temperature, may be construed as an effect of creating nanocomposites. In a nanocomposite material, thermal motion of the tether units is restricted, thereby decreasing the number of organic decomposition pathways accessible to the tether.<sup>19</sup> The char yield, another indicator of thermal stability, also increased upon increasing the OBA-POSS content to 20 wt %, but decreased thereafter—again, similar to the trend in the values of  $T_d$ . For these hybrids, increasing the POSS content appeared to improve the composite's thermal properties through the formation of network structures between the PBZ and the incorporated inorganic silsesquioxane.

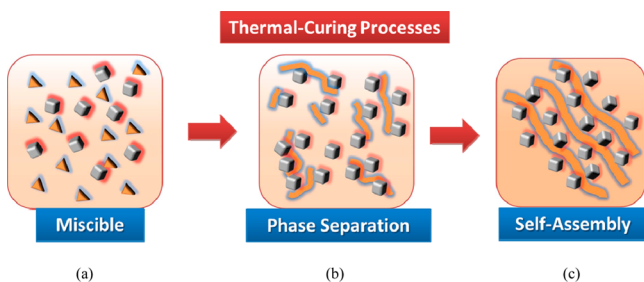
**Self-Assembled Structures of PA-T/OBA-POSS Nanocomposites.** As in a previous study,<sup>12</sup> we found that pure PA-T self-assembled into an alternating packed structure, with a long period of packing of approximately 4.0–4.5 Å, as revealed in the TEM image in Figure 10a. The orientation of the packing (111) is consistent with the presence of T units interacting with the side chains of the PBZ through  $\pi$ - $\pi$  stacking between T layers.<sup>12</sup> Because of the T units in the PBZ matrix, multiple hydrogen bonds formed favorably with A or diaminopyridine units to construct supramolecular structures through simple blending. In addition, OBA-POSS also formed a lamellar structure through the A groups on the corner sites of POSS (Figure 10h and Figure S5). Therefore, we suspected that self-assembly of PA-T/OBA-POSS hybrid materials would lead to interesting structures. Figure 10 displays TEM images PA-T/OBA-POSS nanocomposites incorporating various OBA-POSS contents. At 5 wt % of OBA-POSS, the morphology is similar to that of pure PA-T; we attribute the dark regions to POSS-rich layers because the Si atoms of POSS provide a high mass contrast relative to the organic domain. At 10 and 20 wt % of OBA-POSS, we observe self-assembled lamellar nanostructures (period of ca. 4.5 nm,<sup>20</sup> estimated from Figure S5) in the local region; therefore, we used selected area electron diffraction (SAED) to determine the microstructure. The SAED pattern in Figure S6 (10 wt % of OBA-POSS) reveals a spot pattern, indicating a highly ordered packing structure in the PBZ matrix. Moreover, the four most intense

reflections could be unambiguously identified as  $(2\bar{1}0)$ ,  $(\bar{2}10)$ ,  $(\bar{1}11)$ , and  $(012)$  crystal planes, consistent with the POSS electron diffraction pattern,<sup>21</sup> suggesting that lamellar structures were formed by POSS packing in the PBZ matrix with a preferred orientation along the  $(012)$  plane through A-T interactions between PA-T and OBA-POSS. The TEM images revealed that the nanolamellar structure disintegrated after incorporation of more than 40 wt % of OBA-POSS; the corresponding SAED patterns transformed into ring patterns (inset of Figure 10f), presumably because the self-aggregation of POSS was stronger than the complementary A-T multiple hydrogen bonding interactions and because the ordered structure of POSS packing was disrupted. These observations are consistent with the best fits of the Kwei equation—quite predictable at OBA-POSS contents of less than 40 wt %, but with a divergence of the experimental values of  $T_g$  at OBA-POSS contents greater than 40 wt %, reflecting the disruption of specific interassociation interactions through self-aggregation of OBA-POSS. We suspect that the self-assembled lamellar structures resulted from POSS separating from the matrix and aggregating along a specific orientation; presumably, complementary multiple hydrogen bonded pairs in PA-T/OBA-POSS and the linear-like structure of PA-T also played important roles in determining the structure formed.

Scheme 3 summarizes these possible processes. Initially, PA-T and OBA-POSS were miscible in the uncured benzoxazine; OBA-POSS separated from PA-T during subsequent thermal curing as a result of reaction-induced phase separation.<sup>22</sup> Finally, the self-aggregation of OBA-POSS was restricted through A-T multiple hydrogen bonding interactions with the linear structure of PA-T; it would later occur in the nanosize domains, with growth along the  $(012)$  plane. This morphology is similar to that of the microphase separation of block copolymers in the bulk state<sup>23</sup> and different polymer/POSS nanocomposites.<sup>24</sup>

**Thin Film Properties of PA-T/OBA-POSS Nanocomposites.** Surface properties are important factors influencing the applications of PBZs in, for example, nanoimprint lithography, microelectromechanical systems (MEMS), and superhydrophobic surfaces.<sup>2</sup> Supramolecules have been reported to exhibit good film forming characteristics through noncovalent bonds,<sup>10i,20b</sup> similar to the behavior of our PA-T/OBA-POSS = 80/20 nanocomposite (see Figure S2). Although dynamic mechanical analysis (DMA) is typically used to measure the mechanical properties of PBZs in the bulk state,<sup>7j,k</sup> the corresponding thin film properties are very

**Scheme 3. Possible Self-Assembly through Three Steps:** (a) the PA-T Monomer Is Miscible with OBA-POSS in the Uncured Benzoxazine; (b) OBA-POSS Separates from the Cured PA-T Benzoxazine through a Reaction-Induced Phase Separation Mechanism; (c) Self-Aggregation of OBA-POSS Restricted by Complementary Multiple Hydrogen Bonding Interactions (A–T) and the Linear Structure of PA-T PBZ, Resulting in Self-Assembly of POSS Units through Subsequent Growth along the (012) Plane



difficult to measure. Figure 11 presents the loading–displacement curve of the PA-T and OBA-POSS hybrid incorporating 20 wt %

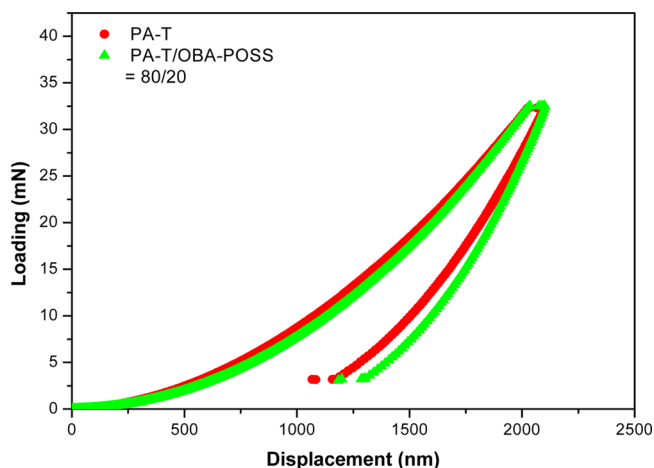


**Figure 11.** Loading–displacement curves of pure PA-T and a PA-T/OBA-POSS thin film.

of OBA-POSS (depth: 200–2000 nm). The modulus of pure PA-T was  $5.09 \pm 0.08$  GPa; its surface hardness was  $0.53 \pm 0.01$  GPa. The modulus of the nanocomposite incorporating 20 wt % of OBA-POSS ( $5.22 \pm 0.06$ ) was higher than that of pure PA-T, but the surface hardness ( $0.45 \pm 0.01$ ) was lower. This phenomenon presumably resulted from opposing effects of reinforcement and cross-linking density in the PBZ matrix. On one hand, the nanoreinforcement effect of OBA-POSS would suppress molecular mobility in the PBZ matrix and tend to increase the modulus; on the other, the inclusion of POSS nanoparticles in the system would decrease the cross-linking density of PBZ.<sup>7j,25</sup> The definition of surface hardness is resistance to deformation on the surface of a material. As a result, a lower cross-linking density would lead to a relatively low surface hardness.

Moreover, Figure S7 indicates the high dispersion of OBA-POSS in the PBZ matrix, with Figure S7a displaying the almost identical loading/unloading curves of six different sites on the surface and Figure S7b revealing the modulus and hardness distributed over the depth of the sample, implying the

homodistribution in our thin film. Therefore, the nanodomains of OBA-POSS were dispersed very well in the PBZ, allowing the preparation of thin films (or coating layers) of PBZ/POSS nanocomposites through multiple hydrogen bonding interactions. The OBA-POSS content in this system increased the strength (high modulus) relative to that of pure PBZ, but the sample could not scratch the surface of a different material (relatively lower hardness).

## CONCLUSIONS

Complementary multiple hydrogen bonding between a well-defined star-shaped A-functionalized POSS and a T-functionalized benzoxazine has resulted in the formation of new supramolecular structures. With a surprising aggregation stability, the self-assembly of alternating lamellar structures resulted from spontaneous association of the complementary components through polycondensation based on multiple hydrogen bonding interactions. This approach might lead to the preparation of a wide range of self-assembled supramolecular structures with properties similar to those from the microphase separation of block copolymers in the bulk state.

## ASSOCIATED CONTENT

### Supporting Information

Additional characterization data (Figures S1–S7). This material is available free of charge via the Internet at <http://pubs.acs.org>.

## AUTHOR INFORMATION

### Corresponding Author

\*E-mail [kuosw@faculty.nsysu.edu.tw](mailto:kuosw@faculty.nsysu.edu.tw).

### Notes

The authors declare no competing financial interest.

## ACKNOWLEDGMENTS

This study was supported financially by the National Science Council, Taiwan, Republic of China, under Contracts NSC 100-2221-E-110-029-MY3 and NSC 100-2628-E-110-001.

## REFERENCES

- (1) (a) Nair, C. P. R. *Prog. Polym. Sci.* **2004**, *29*, 401. (b) Ghosh, N. N.; Kiskan, B.; Yagci, Y. *Prog. Polym. Sci.* **2007**, *32*, 1344. (c) Ishida, H.; Allen, D. J. *J. Polym. Sci., Part B: Polym. Phys.* **1996**, *34*, 1019.
- (2) (a) Vengatesan, M. R.; Devaraju, S.; Dinakaran, K.; Alagar, M. J. *Mater. Chem.* **2012**, *22*, 7559. (b) Yagci, Y.; Kiskan, B.; Ghosh, N. N. *J. Polym. Sci., Part A: Polym. Chem.* **2009**, *47*, 5565. (c) Wang, C. F.; Su, Y. C.; Kuo, S. W.; Huang, C. F.; Sheen, Y. C.; Chang, F. C. *Angew. Chem., Int. Ed.* **2006**, *45*, 2248. (d) Kuo, S. W.; Wu, Y. C.; Wang, C. F.; Jeong, K. U. *J. Phys. Chem. C* **2009**, *113*, 20666. (e) Lin, C. H.; Chang, S. L.; Shen, T. Y.; Shih, Y. S.; Lin, H. T.; Wang, C. F. *Polym. Chem.* **2012**, *3*, 935. (f) Wang, C. F.; Chiou, S. F.; Ko, F. H.; Chen, J. K.; Chou, C. T.; Huang, C. F.; Kuo, S. W.; Chang, F. C. *Langmuir* **2007**, *23*, 5868. (g) Wang, C. F.; Chang, F. C.; Kuo, S. W. *Handbook of Polybenzoxazine*; Ishida, H., Agag, T., Eds.; Elsevier: Amsterdam, 2011; Chapter 33, p 579. (h) Wang, C. F.; Wang, T. F.; Liao, C. S.; Kuo, S. W.; Lin, H. C. *J. Phys. Chem. C* **2011**, *115*, 16495. (i) Li, Q.; Zhong, X. *Langmuir* **2011**, *27*, 8365. (j) Vengatesan, M. R.; Devaraju, S.; Dinakaran, K.; Alagar, M. J. *Mater. Chem.* **2012**, *22*, 7559.
- (3) (a) Ishida, H. *Handbook of Polybenzoxazine*; Ishida, H., Agag, T., Eds.; Elsevier: Amsterdam, 2011; Chapter 1, p 1. (b) Li, X.; Gu, Y. *Polym. Chem.* **2011**, *2*, 2778.
- (4) (a) Chernykh, A.; Agag, T.; Ishida, H. *Polymer* **2009**, *50*, 3153. (b) Agag, T.; Takeichi, T. *Macromolecules* **2001**, *34*, 7257. (c) Agag, T.; Takeichi, T. *Macromolecules* **2003**, *36*, 6010. (d) Kiskan, B.; Yagci, Y. *Polymer* **2008**, *49*, 2455. (e) Kiskan, B.; Aydogan, B.; Yagci, Y. J.

*Polym. Sci., Part A: Polym. Chem.* **2009**, *47*, 804. (f) Chernykh, A.; Agag, T.; Ishida, H. *Macromolecules* **2009**, *42*, 5121. (g) Kuo, S. W.; Liu, W. C. *J. Appl. Polym. Sci.* **2010**, *117*, 3121.

(5) (a) Rimdusit, S.; Ishida, H. *Polymer* **2000**, *41*, 7941. (b) Takeichi, T.; Agag, T.; Zeidam, R. *J. Polym. Sci., Part A: Polym. Chem.* **2001**, *39*, 2633. (c) Li, X.; Xia, Y.; Xu, W.; Ran, O.; Gu, Y. *Polym. Chem.* **2012**, *3*, 1629. (d) Su, Y. C.; Kuo, S. W.; Xu, H. Y.; Chang, F. C. *Polymer* **2003**, *44*, 2187.

(6) (a) Agag, T.; Takeichi, T. *Polymer* **2000**, *41*, 7083. (b) Phirivawirut, P.; Magaraphan, R.; Ishida, H. *Mater. Res. Innovations* **2001**, *4*, 187. (c) Fu, H. K.; Huang, C. F.; Kuo, S. W.; Lin, H. C.; Yei, D. R.; Chang, F. C. *Macromol. Rapid Commun.* **2008**, *29*, 1216.

(7) (a) Zhang, J.; Xu, R.; Yu, D. *Eur. Polym. J.* **2007**, *43*, 743. (b) Chen, Q.; Xu, R.; Zhang, J.; Yu, D. *Macromol. Rapid Commun.* **2005**, *26*, 1878. (c) Liu, Y.; Zheng, S. *J. Polym. Sci., Part A: Polym. Chem.* **2006**, *44*, 1168. (d) Lee, Y. J.; Huang, J. M.; Kuo, S. W.; Chen, J. K.; Chang, F. C. *Polymer* **2004**, *46*, 2320. (e) Lee, Y. J.; Kuo, S. W.; Su, Y. C.; Chen, J. K.; Tu, C. W.; Chang, F. C. *Polymer* **2004**, *45*, 6321. (f) Lee, Y. J.; Huang, J. M.; Kuo, S. W.; Chen, J. K.; Chang, F. C. *Polymer* **2005**, *46*, 2320. (g) Lee, Y. J.; Kuo, S. W.; Huang, C. F.; Chang, F. C. *Polymer* **2006**, *47*, 4378. (h) Huang, J. M.; Kuo, S. W.; Huang, H. J.; Wang, Y. X.; Chen, Y. T. *J. Appl. Polym. Sci.* **2009**, *111*, 628. (i) Wu, Y. C.; Kuo, S. W. *Polymer* **2010**, *51*, 3948. (j) Huang, K. W.; Kuo, S. W. *Macromol. Chem. Phys.* **2010**, *211*, 2301. (k) Huang, K. W.; Kuo, S. W. *Polym. Comp.* **2011**, *32*, 1086. (l) Kuo, S. W.; Chang, F. C. *Prog. Polym. Sci.* **2011**, *36*, 1649.

(8) Chen, Q.; Xu, R.; Yu, D. *Polymer* **2006**, *47*, 7711.

(9) (a) Sherrington, D. C.; Taskinen, K. A. *Chem. Soc. Rev.* **2001**, *30*, 83. (b) Sivakova, S.; Rowan, S. J. *Chem. Soc. Rev.* **2005**, *34*, 9.

(10) (a) Boal, A. K.; Ilhan, F.; DeRouchey, J. E.; Thurn-Albrecht, T.; Russell, T. P.; Rotello, V. M. *Nature* **2000**, *404*, 746. (b) Uzun, O.; Sanyal, A.; Nakade, H.; Thibault, R. J.; Rotello, V. M. *J. Am. Chem. Soc.* **2004**, *126*, 14773. (c) Puskas, J. E.; Dahman, Y.; Margaritis, A.; Cunningham, M. *Biomacromolecules* **2004**, *5*, 1412. (d) Marsh, A.; Khan, A.; Garcia, M.; Haddleton, D. M. *Chem. Commun.* **2000**, 2083. (e) Aida, T.; Meijer, E. W.; Stupp, S. I. *Science* **2012**, *335*, 813. (f) Kuo, S. W.; Cheng, R. S. *Polymer* **2009**, *50*, 177. (g) Kuo, S. W.; Tsai, S. T. *Macromolecules* **2009**, *42*, 4701. (h) Kuo, S. W.; Hsu, C. H. *Polym. Int.* **2010**, *59*, 998. (i) Wu, Y. C.; Kuo, S. W. *J. Mater. Chem.* **2012**, *22*, 2982. (j) Kuo, S. W.; Tsai, H. T. *J. Appl. Polym. Sci.* **2012**, *123*, 3275. (k) Wu, Y. C.; Kuo, S. W. *Polym. Chem.* **2012**, *3*, 3100.

(11) Yen, Y. C.; Cheng, C. C.; Chu, Y. L.; Chang, F. C. *Polym. Chem.* **2011**, *2*, 1648.

(12) Hu, W. H.; Huang, K. W.; Kuo, S. W. *Polym. Chem.* **2012**, *3*, 1546.

(13) Kuo, S. W.; Tsai, H. T. *Polymer* **2010**, *51*, 5695.

(14) (a) Zhang, W. B.; Li, Y.; Li, X.; Dong, X.; Yu, X.; Wang, C. L.; Wesdemiotis, C.; Quirk, R. P.; Cheng, S. Z. D. *Macromolecules* **2011**, *44*, 2589. (b) Lin, Y. C.; Kuo, S. W. *Polym. Chem.* **2012**, *3*, 162. (c) Lin, Y. C.; Kuo, S. W. *Polym. Chem.* **2012**, *3*, 882.

(15) (a) Shen, S.; Torkelson, J. M. *Macromolecules* **1992**, *25*, 721. (b) Luis, C. C.; Jose, R. I.; Katime, I. *Macromolecules* **1994**, *27*, 7887. (c) Chen, X.; An, L.; Li, L.; Yin, J.; Sun, Z. *Macromolecules* **1999**, *32*, 5905. (d) Natansohn, A. *J. Polym. Sci., Polym. Lett. Ed.* **1985**, *23*, 305. (e) Uriarte, C.; Eguiazabal, J. I.; Llanos, M.; Iribarren, J. I.; Iruin, J. J. *Macromolecules* **1987**, *20*, 3038. (f) Kuo, S. W.; Chang, F. C. *Macromol. Chem. Phys.* **2002**, *203*, 868.

(16) (a) Li, D.; Brisson, J. *Macromolecules* **1996**, *29*, 868. (b) Dong, J.; Ozaki, Y. *Macromolecules* **1997**, *30*, 286. (c) Lin, C. L.; Chen, W. C.; Liao, C. S.; Su, Y. C.; Huang, C. F.; Kuo, S. W.; Chang, F. C. *Macromolecules* **2005**, *38*, 6435.

(17) Kwei, T. J. *Polym. Sci., Polym. Lett. Ed.* **1984**, *22*, 307.

(18) (a) Kuo, S. W.; Chang, F. C. *Macromolecules* **2001**, *34*, 5224. (b) Kuo, S. W.; Chang, F. C. *Polymer* **2003**, *44*, 3021. (c) Kuo, S. W.; Shih, C. C.; Shieh, J. S.; Chang, F. C. *Polym. Int.* **2004**, *53*, 218.

(19) (a) Lin, H. C.; Kuo, S. W.; Huang, C. F.; Chang, F. C. *Macromol. Rapid Commun.* **2006**, *27*, 537. (b) Lu, C. H.; Wang, J. H.; Chang, F. C.; Kuo, S. W. *Macromol. Chem. Phys.* **2010**, *211*, 1339. (c) Huang, K. W.; Tsai, L. W.; Kuo, S. W. *Polymer* **2009**, *50*, 4876.

(20) (a) Sheen, Y. C.; Lu, C. H.; Huang, C. F.; Kuo, S. W.; Chang, F. C. *Polymer* **2008**, *49*, 4017. (b) Shih, R. S.; Lu, C. H.; Kuo, S. W.; Chang, F. C. *J. Phys. Chem. C* **2010**, *114*, 12855.

(21) Waddon, A. J.; Coughlin, E. B. *Chem. Mater.* **2003**, *15*, 4555.

(22) Inoue, T. *Prog. Polym. Sci.* **1995**, *20*, 119.

(23) (a) Rodríguez-Hernández, J.; Chécot, F.; Gnanou, Y.; Lecommandoux, S. *Prog. Polym. Sci.* **2005**, *30*, 691. (b) Chen, S. C.; Kuo, S. W.; Jeng, U. S.; Su, C. J.; Chang, F. C. *Macromolecules* **2010**, *43*, 1083.

(24) (a) Wang, J. H.; Cheng, C. C.; Yen, Y. C.; Miao, C. C.; Chang, F. C. *Soft Matter* **2012**, *8*, 3747. (b) Leu, C. M.; Reddy, G. M.; Wei, K. H.; Shu, C. F. *Chem. Mater.* **2003**, *15*, 2261. (c) Leu, C. M.; Chang, Y. T.; Wei, K. H. *Chem. Mater.* **2003**, *15*, 3721.

(25) Kim, K. M.; Keum, D. K.; Chujo, Y. *Macromolecules* **2003**, *36*, 867.